Properties of Gaseous Optical Masers in Weak Axial Magnetic Fields

W. J. TOMLINSON AND R. L. FORK
Bell Telephone Laboratories, Murray Hill, New Jersey

(Received 27 February 1967)

The theory of a gaseous optical maser in a magnetic field, as derived by Sargent, Lamb, and Fork, was compared with experiment for the case of a single-spatial-mode, internal-mirror maser in an axial magnetic field. Under these circumstances the twofold polarization degeneracy of the cavity mode is broken down, and the maser tends to oscillate in the two oppositely circularly polarized components of the mode. The intensities and frequency difference of these two components were measured as functions of cavity length and magnetic field for $J=1\rightarrow J=0$ and $J=1\rightarrow J=2$ transitions in He-Ne optical masers. It was found that all of the qualitative features of the results were correctly predicted by the theory, and in many cases excellent quantitative agreement was found between theory and experiment. Two areas of disagreement were found. (1) The coupling between the two polarizations is somewhat stronger than that predicted by theory. This is very clear for a $J=1\rightarrow J=0$ transition, and may be present in the $J=1\rightarrow J=2$ transition. No completely satisfactory explanation of this effect has been given. (2) The calculated frequency difference for the $J=1\rightarrow J=2$ transition appears to be smaller than that found in the experiment, although theory and experiment are in good agreement for the $J=1\rightarrow J=0$ transition. The effects, of small anisotropies in the cavity, on both the intensities and frequency difference were studied, and it was found that the theoretical results are in excellent agreement with experiment.

I. INTRODUCTION

A COMPREHENSIVE theory of optical masers in magnetic fields has recently been published by Sargent, Lamb, and Fork.[1] The purpose of this paper is to examine some of the detailed predictions of this theory and to compare these predictions with experiment. Although the theory is able to handle, among other things, an arbitrary number of cavity modes, arbitrary orientations of the magnetic field, and rather general cavity anisotropies, the present experiments have been restricted to a single spatial mode of the cavity, to magnetic fields along the axis of the maser, and to internal-mirror cavities with relatively small polarization bias. Other field orientations and large cavity-anisotropies, such as Brewster-angle windows, will be the subject of subsequent experiments.

The primary concern in this work has been the qualitative comparison of theory and experiment, although these comparisons are more quantitative than previous work. A certain amount of parameter variation was carried out to improve the quantitative agreement and to determine if the required values of the parameters were consistent with those obtained by other methods. However, no extensive "curve fitting" was attempted. Since the available theory only includes terms through third order in the electric field amplitudes, and the experiments were usually done at comparatively high values of the relative excitation (typically $\mathfrak{N}\approx 1.2$), one expects small quantitative differences between the theory and experiment.[2] A more serious problem is that the present theory does not include the effects of atomic collisions. Although some of these effects can be accounted for by relatively simple phenomenological additions to the theory,[3,4] there appear to be other effects which cannot be so handled.[5,6] At such time as a theory is available which includes a more basic treatment of collision effects, a curve-fitting program will be much more attractive.[7]

In the next section we summarize the relevant theoretical expressions from Papers I and II and discuss the procedures used in the calculations. Because of the complexity of the phenomena, and the close relationship between the experimental and theoretical investigations, the major portion of the paper is subdivided by phenomena, rather than into the traditional theory, experiment, and discussion sections. Sections III and IV cover, respectively, the mode intensities, and the beat frequency between the modes. In both cases the effects of cavity anisotropies are neglected. In Sec. V we consider the effects of such anisotropies. To keep the main text to readable length, the details of the experimental techniques have been placed in an Appendix. Since a rather complete annotated bibliography can be found in (I–IX), we only refer to those papers which illustrate particular points.

II. BASIC THEORY

The basic result of the theory derived in Paper I is a set of coupled, nonlinear, first-order differential

[1] M. Sargent III, W. E. Lamb, Jr., and R. L. Fork, first preceding paper, Phys. Rev. **164**, 436 (1967); second preceding paper, Phys. Rev. **164**, 450 (1967); referred to as Papers I and II. When referring to these papers we will indicate the relevant paper and section or equation. For example, (II-V) refers to Paper II, Sec. V, and (I-57) refers to Paper I, Eq. (57).

[2] K. Uehara and K. Shimoda, Japan. J. Appl. Phys. **4**, 921 (1965).

[3] R. L. Fork and M. A. Pollack, Phys. Rev. **139**, A1408 (1965).

[4] A. Szöke and A. Javan, Phys. Rev. **145**, 137 (1966).

[5] R. L. Fork, W. J. Tomlinson, and L. J. Heilos, Appl. Phys. Letters **8**, 162 (1966).

[6] R. L. Fork and W. J. Tomlinson, IEEE J. Quantum Electron. **QE-2**, 23 (1966).

[7] A theory of the optical maser with pressure effects has been derived by B. L. Gyorffy and W. E. Lamb, Jr. (to be published), but it does not include the effects of a magnetic field.

equations which describe the time behavior of the electric field amplitudes, frequencies, and phases. The theory is an extension of the well-known Lamb theory of the optical maser,[8] except that instead of a two-level system one must consider $(2J_a+1)+(2J_b+1)$ levels where J_a and J_b are the angular momenta of the atomic states involved in the maser transitions, and since the twofold polarization degeneracy of the cavity modes is removed by the magnetic field, for each cavity mode above threshold one must consider two polarization modes. Magnetic field effects on the dynamics of the discharge are assumed to be negligible, and for the field strengths we have used this is a very good assumption.

For particular orientations of the magnetic field the theory is *comparatively* simple, provided we use the appropriate representation for the electric field, and the cavity anisotropy is sufficiently small. We consider here the simplest case: a magnetic field parallel to the axis of the maser, with the electric field in terms of opposite circular polarizations. More than one spatial mode of the cavity could have been included, but it appeared that this would only have complicated both the calculations and the experiments without adding significantly to our understanding of the maser. Since we will be primarily concerned with a single spatial mode of the maser cavity we will use the words "modes" or "polarizations" to indicate the two circularly polarized components of the same spatial mode. When more than one spatial mode of the cavity is intended this will be specifically stated.

The basic equations describing a single-cavity-mode maser in an axial magnetic field are[1]

$$\dot{E}_+=\alpha_+E_+-\beta_+E_+^3-\theta_+{}_-E_+E_-^2 - (Q_{xy}\cos\psi-\nu_{xy}\sin\psi)E_-, \quad (1)$$

$$\dot{E}_-=\alpha_-E_--\beta_-E_-^3-\theta_-{}_+E_-E_+^2 - (Q_{xy}\cos\psi+\nu_{xy}\sin\psi)E_+, \quad (2)$$

$$\nu_++\dot{\varphi}_+=\Omega+\sigma_++\rho_+E_+^2+\tau_+{}_-E_-^2 + (Q_{xy}\sin\psi+\nu_{xy}\cos\psi)E_-/E_+, \quad (3)$$

$$\nu_-+\dot{\varphi}_-=\Omega+\sigma_-+\rho_-E_-^2+\tau_-{}_+E_+^2 - (Q_{xy}\sin\psi-\nu_{xy}\cos\psi)E_+/E_-, \quad (4)$$

$$\dot{\psi}=\nu_++\dot{\varphi}_+-\nu_--\dot{\varphi}_-. \quad (5)$$

In these equations E_+ and E_- are the amplitudes of the electric fields in the two polarization modes, ν_+ and ν_- are their frequencies, and φ_+ and φ_- are their phases. The plus subscript refers to the polarization which has its angular momentum in the same direction as a positive magnetic field. The terms involving Q_{xy} and ν_{xy} represent, respectively, linearly polarized loss anisotropy, and linear birefringence. These quantities can be written in the forms $Q_{xy}=(l_x-l_y)\Delta/2$, and $\nu_{xy}=(\varphi_x-\varphi_y)\Delta/2$, where l_x and l_y are the cavity losses for light linearly polarized along the x and y axes, φ_x and φ_y are the corresponding phase shifts, and $\Delta=c/2L$ is the cavity mode spacing. (The cavity length is L, and c is the velocity of light.) The unperturbed cavity resonance frequency Ω is assumed to be the same for the opposite circular polarizations. The α's, β's, θ's, σ's, ρ's, and τ's are complicated functions of the atomic level parameters, magnetic field, excitation conditions and cavity tuning, and can be found in (II-13)–(II-26). These coefficients also depend on the frequency difference of the modes, but the dependence is so weak that it is usually neglected. The quantity $(l_x+l_y)\Delta/2$ appears as a scale factor in all the coefficients, but this is of importance only when we consider absolute frequency measurements, and will be discussed in Sec. IV.

Numerical evaluations of these equations were done using the computer programs described in (I–VIII). Although some changes were made in the programs to facilitate the particular calculations of interest, the mathematics were left unchanged. The reader is referred to Papers I and II for a more complete discussion of the programs. We will here simply summarize the parameters which must be specified before the program can provide numerical results. The parameters of the atomic levels which must be specified are: J_a, the total angular momentum of the upper state; g_a, the g value of the upper state; γ_a, the reciprocal radiative lifetime of the upper state; similarly J_b, g_b, and γ_b for the lower state; γ_{ab}, the natural linewidth of the transition (γ_{ab} is used as an independent parameter to allow for collision effects);[3] and Ku, the Doppler-width constant.[8] The parameters of the maser which must be specified are: $\mathfrak{N}$, the relative excitation[8] ($\mathfrak{N}=1$ at threshold); Δ, the cavity longitudinal mode spacing; l, the single-pass cavity loss; $\Omega-\omega_0$, the difference between the cavity resonance frequency and the atomic line center; and H, the magnetic field. For an anisotropic cavity we must also specify l_x-l_y, and $\varphi_x-\varphi_y$ as described above. In addition, the program has several other options. An asymmetry in the atomic interaction curve of the type used in Ref. 3 can be included. The relative excitations of the magnetic sublevels can be specified individually to account for unequal pumping of the sublevels, and different losses can be used for the two polarizations. The integrals involved in the third-order terms can be evaluated using a δ-function approximation or Doppler limit,[8] or, at the expense of additional computing time, they can be evaluated exactly.[1] For the cases presented in this paper the error resulting from use of the δ-function approximation is rather small, but as indicated in the figure captions most of the data which are presented were calculated with the exact expression for the integrals. Finally, the dependence of the coefficients on the frequency difference of the modes can be handled by an iterative calculation, but it has been found that this is such a small correction ($\sim$1 part in 10^3) that it was usually neglected.

[8] W. E. Lamb, Jr., Phys. Rev. **134**, A1429 (1964).

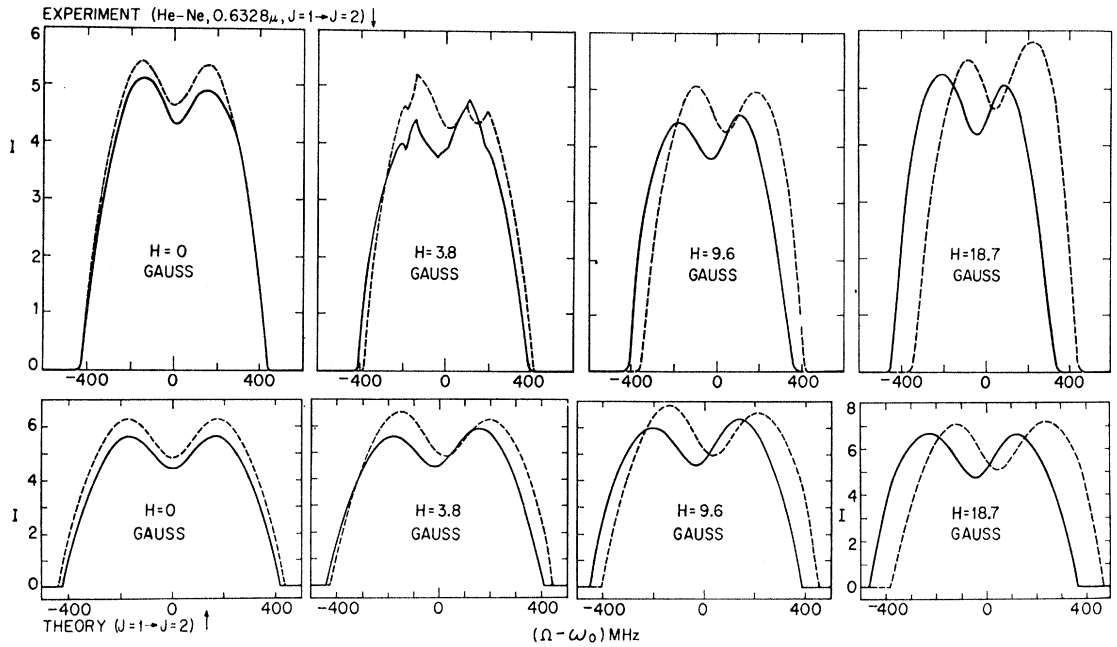

FIG. 1. Experimental and theoretical curves of polarization mode intensities as functions of cavity detuning for a $J=1\rightarrow J=2$ transition for several values of axial magnetic field. The experimental curves are from an internal-mirror He^3-Ne^{20} maser operating on the $3s_2-2p_4$ ($J=1\rightarrow J=2$) transition of Ne at 0.6328 μ. The discharge was dc-excited, and the total gas pressure was 2.1 Torr with $He^3:Ne^{20}=7:1$. The bumps in the 3.8-G experimental curves at ± 200 MHz are a consequence of cavity anisotropy effects which were not included in these calculations (see Sec. V for a discussion of this phenomena). For the theoretical calculations $J_a=1$, $J_b=2$, $g_a=g_b=1.3$, $\gamma_a/2\pi=18$ MHz, $\gamma_b/2\pi=40$ MHz, $\gamma_{ab}/2\pi=120$ MHz, $Ku=1010$ MHz. To improve the agreement with the experiment the populations of the magnetic sublevels were adjusted so that for the transitions for which $m_a-m_b=+1$ the relative excitation was $\mathfrak{N}_+=1.178$, while for $m_a-m_b=-1$ the relative excitation was $\mathfrak{N}_-=1.172$. The third-order integrals were evaluated exactly. For all cases the dashed curve is E_+^2 and the solid curve is E_-^2. All intensities are in arbitrary units. The same intensity scale factor was used for all the theoretical curves so one can compare their intensities for different field values, but small variations in the relative excitation during the course of the experiment make such comparisons invalid for the experimental curves.

As they are written, Eqs. (1) to (5) are rather formidable, even if we ignore the fact that the coefficients in the equations are themselves complicated functions of the basic maser parameters. To make it easier to understand the implications of these equations we assume, in Secs. III and IV, that the cavity anisotropies are sufficiently small that we can neglect terms involving Q_{xy} and ν_{xy}. In this case there are stationary solutions for the mode amplitudes and frequencies which we will examine in some detail and compare with experimental results. We will then, in Sec. V, include the effects of the cavity anisotropy (Q_{xy} and/or $\nu_{xy}\neq 0$).

III. MODE AMPLITUDES FOR $Q_{xy}=\nu_{xy}=0$

If we consider only mode amplitudes and assume $Q_{xy}=\nu_{xy}=0$, we have a somewhat simpler set of equations to deal with

$$\dot{E}_+=E_+(\alpha_+-\beta_+E_+^2-\theta_{+-}E_-^2), \tag{6}$$

$$\dot{E}_-=E_-(\alpha_--\beta_-E_-^2-\theta_{-+}E_+^2). \tag{7}$$

In these equations it is easy to see that the α terms represent the net unsaturated gains for the two modes, the β terms represent the saturation of each mode by itself, and the θ terms represent the saturation of each mode by the other mode or mode coupling. (An interpretation of these coefficients in terms of various physical processes can be found in Ref. 9.) Equations (6) and (7) describe the time evolution of the maser intensities, but since for most initial conditions the intensities rapidly (in times of the order of 100 μsec or less) approach equilibrium values, in this section we need only concern ourselves with these equilibrium solutions. In (II–III) an algorithm is given for determining the equilibrium solutions from the values of the coefficients in the equations. If the coupling between the modes is weak ($\theta_{+-}\theta_{-+}<\beta_+\beta_-$) the maser can exhibit either one- or two-mode operation. If the coupling is strong ($\theta_{+-}\theta_{-+}>\beta_+\beta_-$) the maser can only exhibit one-mode operation, but in some cases it will be bistable so that either mode can oscillate and the oscillating mode is determined by the past history of the maser.

As a simple example of the effects of the magnetic field on the mode intensities let us consider a $J=\frac{1}{2}\rightarrow J=\frac{1}{2}$ transition for which $\theta_{+-}=\theta_{-+}=0$ so there is no

[9] R. L. Fork and M. Sargent III, in *Proceedings of the International Conference on the Physics of Quantum Electronics*, edited by P. L. Kelley, B. Lax, and P. E. Tannenwald (McGraw-Hill Book Company, Inc., New York, 1966), pp. 611–619.

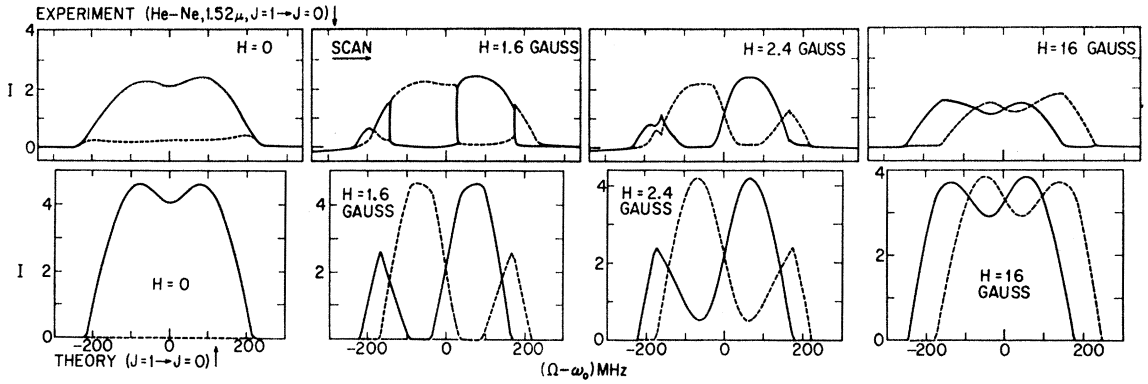

FIG. 2. Experimental and theoretical curves of polarization mode intensities as functions of cavity detuning for a $J=1\rightarrow J=0$ transition for several values of axial magnetic field. The experimental curves are from an internal-mirror He^3-Ne^{20} maser operating on the $2s_2-2p_1$ transition of Ne at 1.52 μ. The discharge was dc-excited, and the total gas pressure was 2.2 Torr with $He^3:Ne^{20}=10:1$. The maser was bistable, with respect to oscillating mode, over portions of the 1.6-G curves and over the zero-field curves (see text for further details). The bumps in the experimental curves, such as those at -180 MHz in the 2.4-G curves, are a consequence of cavity anisotropy effects discussed in Sec. V. For the theoretical calculations $J_a=1$, $J_b=0$, $g_a=1.3$, $\gamma_a/2\pi=24$ MHz, $\gamma_b/2\pi=62$ MHz, $\gamma_{ab}/2\pi=81$ MHz, $Ku=460$ MHz, $\mathfrak{N}=1.2$. The third-order integrals were evaluated using the δ-function approximation. For all cases the dashed curve is E_+^2 and the solid curve is E_-^2, in arbitrary units. (See Fig. 1 caption for a discussion of the intensity scale factors.)

coupling between the modes. For zero magnetic field both modes would oscillate with equal intensities, and the tuning curve (curve of intensity as a function of cavity detuning) would show the familiar Doppler-broadened profile with a Lamb dip at the atomic line center.[8] For a nonzero magnetic field the tuning curve would be split into two identical curves, one for each polarization, displaced symmetrically about the line center by an amount proportional to the magnetic field. For transitions with other J values the θ's are nonzero so there is mode coupling or competition. The extent of the departures from the simple behavior of the $\frac{1}{2}\rightarrow\frac{1}{2}$ case depends on the strength of the coupling between the modes.

For transitions of the type $J\rightarrow J+1$ or $J+1\rightarrow J$ for $J\geq\frac{1}{2}$ (we use the notation: upper state $J\rightarrow$lower state J) the coupling is quite weak ($\theta\leq\frac{2}{3}\beta$) so that the behavior of masers operating on such transitions is similar to that described above for a $\frac{1}{2}\rightarrow\frac{1}{2}$ transition. A good example of this is the $3s_2-2p_4$ transition in Ne ($J=1\rightarrow J=2$) at 0.6328 μ as shown in Fig. 1. This figure shows the experimental and theoretical intensities of the two circular polarizations as functions of cavity tuning for several values of the magnetic field. (Details of the experimental procedure can be found in the Appendix. The bumps in the 3.8-G experimental curves at ± 200 MHz are a consequence of frequency-locking phenomena caused by cavity anisotropy which was not included in these calculations, but which will be discussed in Sec. V.) It is easy to see that the major effect of the magnetic field is to split the tuning curve into two curves which move apart as a function of magnetic field.

For the initial theoretical calculations we used the values of the effective decay constants, appropriate to our operating pressure, as obtained by Fork and Pollack,[3] and assumed equal excitations for the magnetic sublevels of each state. These calculations gave the general shapes of the experimental curves but did not reproduce the asymmetries of the experimental results. Further calculations were made assuming small differences in the populations of the magnetic sublevels. The lower half of Fig. 1 shows these results for population differences such that the plus polarization has a relative excitation of $\mathfrak{N}_+=1.178$, and the minus polarization has $\mathfrak{N}_-=1.172$. This difference in gains has the effect of increasing the intensity of the plus polarization relative to the minus polarization, and the coupling between the modes then gives a further asymmetry. We see from the figure that these calculations qualitatively reproduce the asymmetries observed in the experimental results. Population differences of this type are not implausible since the dc discharge current defines a direction. Furthermore, any differences in cavity losses for the two circular polarizations would effect the maser in the same manner. Evidence for these effects was presented in a preliminary letter.[5] It is also possible that some of the asymmetry is a result of cavity anisotropy (see Sec. V). The experimental curves still imply somewhat more coupling than the theoretical curves; however, much more definite evidence for such an effect has been found in other transitions and will be discussed below. We could undoubtedly have obtained a better quantitative fit between theory and experiment by adjusting the atomic constants used in the calculations, and by using a different set of sublevel populations for each magnetic field value. Nevertheless, except for the cavity anisotropy effects which will be discussed in Sec. V, all of the qualitative features of the experimental results are predicted by the theory, and for reasonable values of the constants even the quantitative fit is quite good.

Transitions of the type $J=1\rightarrow J=0$, $J=0\rightarrow J=1$, and $J=1\rightarrow J=1$ form a unique set in that for zero

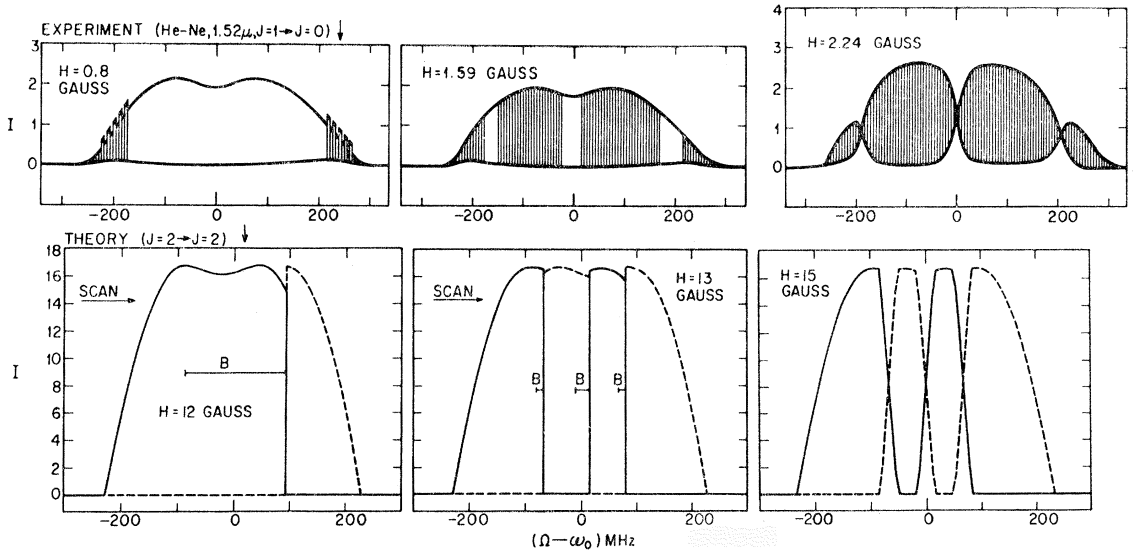

FIG. 3. Experimental and theoretical curves of polarization mode intensities as functions of cavity detuning showing a transition from strong to weak coupling. As the experimental curves were recorded the magnetic field direction was reversed about every 5 MHz. This produces a switchover in mode intensities when the modes are weak-coupled, but not when the maser is in a bistable region. These switchovers have been indicated schematically in the figures by vertical lines. In the 0.8-G curves we have tried to indicate the type of asymmetry which was observed in this case, although it has been necessary to exaggerate the effect by about a factor of 2 to make it clear in the figure. The experimental curves are from the same maser used for Fig. 2 except that for these curves the total gas pressure was 1.9 Torr. The theoretical curves are intended to show the type of behavior predicted by the theory for a strong-coupled transition. The curves have been plotted for a cavity scan in the direction of increasing frequency, and bistable regions are indicated by the horizontal bars marked "B." For these calculations $J_a=J_b=2$, $g_a=g_b=1.3$, $\gamma_a/2\pi=30$ MHz, $\gamma_b/2\pi=60$ MHz, $\gamma_{ab}/2\pi=100$ MHz, $Ku=420$ MHz, $\mathfrak{N}=1.2$. The third-order integrals were evaluated using the δ-function approximation.

magnetic field the theory predicts $\theta_{+-}=\theta_{-+}=\beta_+=\beta_-$, or neutral coupling. For all nonzero fields the coupling is predicted to be weak, and to decrease in strength with increasing magnetic field [see (II–1)]. Therefore, for sufficiently high values of the magnetic field we expect the same type of behavior as we have just seen for a $J=1\rightarrow J=2$ transition, but as the field decreases we expect to see increasing coupling between the modes such that one mode gains intensity at the expense of the other mode.

Figure 2 shows experimental and theoretical results on the mode intensities as a function of cavity tuning for the $2s_2-2p_1(J=1\rightarrow J=0)$ transition of Ne at 1.52 μ. Considering the theoretical curves in order of decreasing field we see that for a field of 16 G the tuning curves are very similar to those considered above, but for a field of 2.4 G the results of the increased coupling are readily apparent. At 1.6 G the coupling is strong enough that on either side of line center the dominant mode quenches the other mode. This leads to three "crossover regions" where the modes interchange intensities over relatively small tuning ranges. For further reductions in the magnetic field the calculated curves are very similar to the 1.6-G curves except that the crossover regions become narrower and approach zero width for zero field. For sufficiently small fields the widths of the crossover regions appear to be directly proportional to the magnetic field, and the constants of proportionality are functions of the various parameters used in the calculations. For zero field the theory predicts a neutral equilibrium with an infinity of acceptable solutions, sometimes referred to as polarization "indifference" [see (II–33)]. In the figure we have shown the solution with only one mode oscillating. All zero-field solutions have the same total intensity.

The experimental curves for 16 G show reasonably good agreement with the theoretical calculation, and the 2.4-G curves show the expected increased coupling, but the experiment implies a coupling somewhat stronger than that predicted by the theory. (The bumps at −180 MHz and the asymmetry in the 2.4-G experimental curves are a consequence of cavity anisotropy and will be discussed in detail in Sec. V). In the experimental curves for 1.6 G we find an unexpected phenomenon. The crossover regions have gone to zero width, and been replaced by regions of bistable operation,[5,6,10] thus implying that the coupling has increased to the point of strong coupling ($\theta_{+-}\theta_{-+}>\beta_+\beta_-$). In the figure, which is for a tuning scan in the direction of increasing cavity frequency, the central crossover region is essentially a point and occurs about 25 MHz to the high-frequency side of line center. For a tuning scan in the opposite direction this crossover appeared about 25 MHz below line center, so for this field value we have a bistable region about 50 MHz wide at line center.

[10] Strong coupling of this transition at zero field was observed independently by H. De Lang and G. Bouwhuis (Ref. 12), but they have not reported results for other field values.

Similar regions exist at the outer crossovers as will be demonstrated below. For zero magnetic field the coupling is strong across the entire tuning curve and we obtain essentially single-mode, bistable operation. (The observed finite intensity of the mode which is "out" is another consequence of cavity anisotropy to be covered in Sec. V.)

Because this strong coupling was not predicted by theory, a number of measurements were made to determine its properties. To show the approach to strong coupling, measurements were made of the widths of the crossover regions as a function of magnetic field. These showed a linear dependence on magnetic field as predicted by theory, and had about the same slope as the theoretical curves, but the experimental widths went to zero at a field of about 2 G, rather than at zero field as predicted by the theory. To show the bistable regions more clearly, tuning curves were recorded while the direction of the magnetic field was being rapidly reversed. In weak-coupled regions this produced a series of vertical lines as the modes interchanged intensities. In bistable regions the same mode can oscillate for either direction of the magnetic field and there is no such interchange of intensities. This is shown in the top line of Fig. 3 where we see that bistable regions (light areas) develop about all three crossover points, and as the magnetic field is decreased the bistable regions expand until they join and fill the entire tuning curve. Although the present theory cannot account for strong coupling for a $J=1\rightarrow J=0$ transition, it does predict strong coupling for other transitions. The bottom line of Fig. 3 shows theoretical tuning curves for a $J=2\rightarrow J=2$ transition for field values which bracket the change from strong to weak coupling. The curves are calculated for a tuning scan from low to high frequencies, and the bistable regions are indicated by the horizontal bars marked "*B*." The figures show the same qualitative behavior as we have observed experimentally for the $J=1\rightarrow J=0$ transition. One should not try to draw too many conclusions from this comparison, but it appears safe to say that the primary disagreement between theory and experiment is simply the strength of the coupling between the two polarizations.

In a search for possible mechanisms for this increased coupling, we have attempted to restate, in more physical terms, the theoretical result that the zero-field coupling depends only on the J values of the transition [see (II-34) (II-35)]. If one examines the relative values of the angular matrix elements for the various sublevel transitions for different J values, one finds that for $\Delta J=\pm 1$ the largest matrix element is always for a $\Delta m=\pm 1$ transition while for $\Delta J=0$ the largest matrix element is for a $\Delta m=0$ transition (the only exception is $J=\frac{1}{2}\rightarrow J=\frac{1}{2}$). The sum of the squares of the $\Delta m=0$ matrix elements is always equal to the sum of the squares of the $\Delta m=+1$ or $\Delta m=-1$ matrix elements, giving equal unsaturated gains for either case. However, the saturation depends on the fourth and higher powers

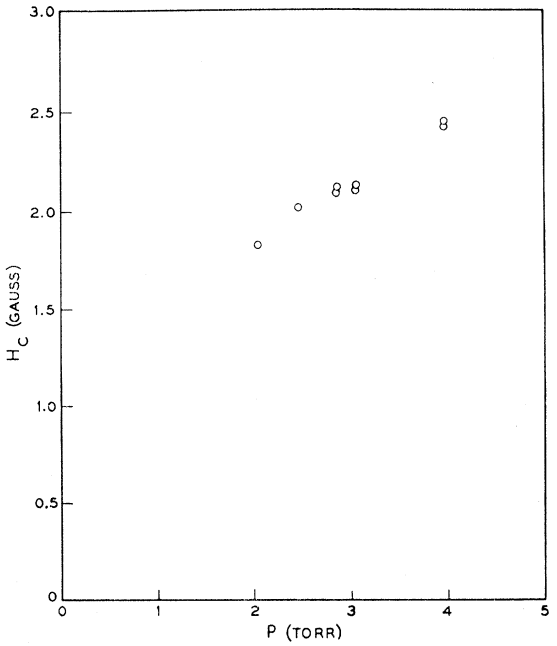

FIG. 4. Critical axial magnetic field H_c as a function of pressure. The critical magnetic field is the field necessary to break down the strong coupling of the two polarization modes. The data are from an internal-mirror He^3-Ne^{20} maser operating on the $2s_2$-$2p_1$ transition of Ne at 1.52 μ. The discharge was dc-excited and the gas partial pressures were in the ratio He^3:$Ne^{20}=10:1$. The pressure indicated on the figure is the total pressure. All the data are for relative excitation $\mathfrak{N}\approx 1.2$, but no strong dependence of H_c on $\mathfrak{N}$ was observed.

of the matrix elements, thus for $\Delta J=\pm 1$ the $\Delta m=0$ transitions (linear polarization) will have the greatest saturated output power, while for $\Delta J=0$ the $\Delta m=\pm 1$ transitions (circular polarization) will have the greatest saturated output power. For the neutral coupled transitions, $J=1\leftrightarrow J=0$ and $J=1\leftrightarrow J=1$, all the matrix elements are identical, so the saturated output power is independent of polarization. We can postulate, therefore, that the coupling strength is a manifestation of a maximum power principle, since the maser always chooses the polarization state which maximizes the total output power.

Collisions are expected to cause transitions between magnetic sublevels tending to equalize the sublevel populations, so in general they would have the effect of driving the coupling closer to neutral (as observed for the $J=1\rightarrow J=2$ transition). A possible explanation of the extra coupling observed for the $J=1\rightarrow J=0$ transition is that the collisions may be more effective in causing $|\Delta m|=2$ transitions (electric quadrupole) than $|\Delta m|=1$ transitions (magnetic dipole), since both transitions assist the circular polarization, but only the latter is important for linear polarization. It appears plausible that $|\Delta m|=2$ collisions are important, since it has been shown[9] that the saturation induces an electric quadrupole moment in the atom, as well as a magnetic dipole moment.

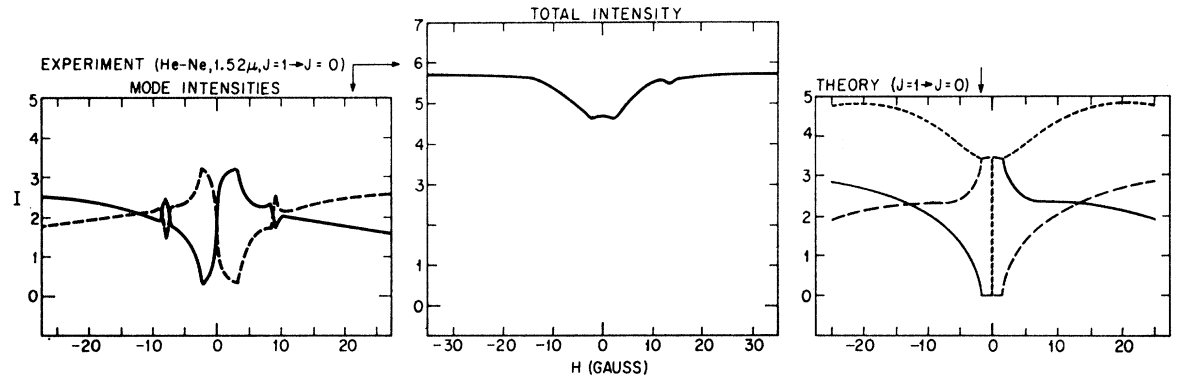

FIG. 5. Experimental and theoretical curves of polarization mode intensities and total intensity as functions of the axial magnetic field strength for a $J=1\rightarrow J=0$ transition with the cavity tuned 75 MHz above the atomic-line center. The experimental curves are from the same maser used for Fig. 2 except that the total gas pressure was 2.1 Torr. For the mode intensities the dashed curve is E_+^2, the solid curve is E_-^2, and the dotted curve is the theoretical total intensity (all in arbitrary units). The constants used in the theoretical calculations were: $J_a=1$, $J_b=0$, $g_a=1.3$, $\gamma_a/2\pi=30$ MHz, $\gamma_b/2\pi=60$ MHz, $\gamma_{ab}/2\pi=100$ MHz, $Ku=420$ MHz, $\mathfrak{N}=1.15$. The third-order integrals were evaluated exactly.

To investigate this suggestion for the origin of the additional coupling for the $J=1\rightarrow J=0$ transition, we measured the critical magnetic field for which the cross-over regions just disappear, as a function of the total gas pressure in the maser. These measurements tell us how much magnetic field is necessary to reduce the coupling from strong to neutral, and in Fig. 4 we see that there is a definite pressure dependence. These results suggest that collision processes in the gas play a role in increasing the coupling. It is possible, however, that the observed pressure dependence is simply the result of the pressure effects on the atomic-level widths. This question could probably be resolved by a series of careful measurements of the pressure dependence of these widths.

For a sufficiently large magnetic field the Zeeman splitting can be made of the order of the cavity mode spacing so the two polarizations oscillate on adjacent longitudinal modes. (We assume that the relative excitation is low enough that each polarization can oscillate on one and only one cavity mode.) The theory predicts that the polarization intensities should essentially behave as if they were on the same mode with a field $(H-H_m)$, where H is the actual field and H_m is the field which produces a splitting equal to the mode spacing. The only difference is that since the electric fields in the two modes are out of phase over the central region of the cavity, where the discharge tends to be concentrated, they partially cancel some of the terms in the θ and τ coefficients, thus decreasing the coupling between the modes. Kannelaud and Culshaw[11] have done experiments on the $J=1\rightarrow J=0$ Xe transition at 2.65 μ which they find to be strong-coupled for zero field and weak-coupled for a field of H_m, but since they do not give the distribution of the discharge in their cavity it has not been possible to determine from their data if the high-field coupling is stronger than that predicted by the theory.

Although Fig. 2 shows a considerable disparity between experiment and theory, a small additional coupling in the theory would bring it into qualitative agreement with experiment. We did not attempt to make such a correction on a phenomenological basis since we did not have any sound theoretical guidance as to the form that such a correction should take. Therefore, there was no point in attempting to vary the parameters in the calculations to improve the fit with experiment.

The theory predicts that all transitions of the type $J\rightarrow J$ for $J\geq\frac{3}{2}$ are strong-coupled at zero magnetic field, but become weak-coupled for a Zeeman splitting of the order of the smaller of the natural-level widths. Although we have not carried out experiments on any transition of this type, we have observed strong coupling in our experiments on the $J=1\rightarrow J=0$ transition. De Lang and Bouwhuis[12] have examined the $2s_5-2p_6$ transition in Ne $(J=2\rightarrow J=2)$ at 1.207 μ and found the expected strong coupling at zero field, but they have not reported any results for other field values.

Thus far we have considered mode amplitudes as functions of cavity tuning for fixed values of the magnetic field, although we could equally well have plotted the intensities as functions of magnetic field with the cavity tuning held constant. In principle these two procedures give us the same information, but in practice they have different uses. We have seen that the tuning scan is very useful for demonstrating the coupling between the modes, and it is particularly convenient experimentally since the magnetic field is easily held at a constant and reproducible value. Magnetic field scans are useful for the determination of the atomic-level parameters, as discussed in (II-VIII),[13] but are

[11] J. Kannelaud and W. Culshaw, Appl. Phys. Letters **9**, 120 (1966). This paper contains references to previous work by these authors.

[12] H. De Lang and G. Bouwhuis, Phys. Letters **20**, 383 (1966).

[13] H. R. Schlossberg and A. Javan, Phys. Rev. Letters **17**, 1242 (1966).

somewhat less convenient experimentally because of the difficulty of holding the cavity frequency at a constant and reproducible value. Because of this difficulty, and because our purpose in these experiments was a comparison of theory with experiment rather than detailed measurements of atomic constants, we will consider here only one particular case of a magnetic field scan.

Figure 5 shows experimental and theoretical curves of mode intensities and total intensity as functions of magnetic field for a $J=1\rightarrow J=0$ transition with the cavity tuned approximately 75 MHz above the atomic line center. As is shown in (II–VIII), this detuning is sufficient to virtually eliminate the effects of the standing waves in the maser, so the observed dip in the intensity is a pure magnetic tuning dip, or "magnetic Lamb dip." The basic features of the experimental curves are predicted by the theory, but in this case there are rather severe perturbations from cavity anisotropy effects which were not included in the theoretical calculations. These perturbations lead to the rapid variations in mode intensities at ± 9 G, and to the gradual change-over of mode intensities about zero field rather than the abrupt change predicted by the theory. These effects tend to cancel in the total intensity so that there the agreement between experiment and theory is much better. (For the higher-field experiments suggested in (II–VIII) the mode frequencies would be sufficiently far apart that the effects of the cavity anisotropy would be considerably reduced.) It is shown in (II–VIII) that the width of the dip in the total intensity is closely related to γ_a. From the data in the figure we obtain the result $\gamma_a/2\pi=27\pm 5$ MHz at a total pressure of 2.1 Torr (Ne $2s_2$ level, He:Ne partial pressures = 10:1).

Our results on the mode intensities show that the principal discrepancy between theory and experiment is the observation of strong coupling in the $J=1\rightarrow J=0$ case where the theory predicts neutral coupling, and that there is evidence of increased coupling in transitions for which the theory predicts weak coupling. There is no definite evidence, but it appears possible that this coupling effect is a result of atomic collisions in the maser medium. In general the theory has been most successful in predicting the many varied and complex details of the experimental results. Not only are the qualitative features predicted correctly, but except for situations where the extra coupling has a large effect, the quantitative agreement has been very good. Although in this section we have neglected the effects of cavity anisotropy, we will consider them in Sec. V where the theory is shown to be equally successful in predicting these effects.

IV. MODE FREQUENCIES FOR $Q_{xy}=\nu_{xy}=0$

For an isotropic cavity ($Q_{xy}=\nu_{xy}=0$), the equations for the oscillation frequencies of the two modes are

$$\nu_+ + \dot{\varphi}_+ = \Omega + \sigma_+ + \rho_+ E_+^2 + \tau_+ {}_- E_-^2, \quad (8)$$

$$\nu_- + \dot{\varphi}_- = \Omega + \sigma_- + \rho_- E_-^2 + \tau_- {}_+ E_+^2. \quad (9)$$

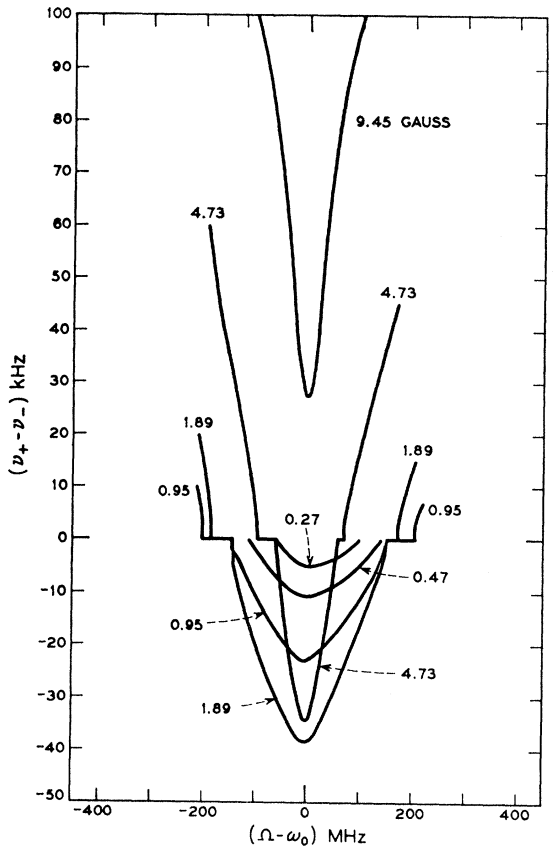

FIG. 6. Experimental curves of the frequency difference between the oppositely circularly polarized modes, as functions of cavity detuning, for several values of axial magnetic field. The data are from the same maser used to obtain the data for Fig. 1 (He–Ne, 0.6328 μ, $J=1\rightarrow J=2$), except that the total gas pressure was 2.1 Torr. The method used to determine the absolute sign of the frequency difference is described in the Appendix. The breaks in the curves as they pass through zero frequency are the result of frequency-locking caused by cavity anisotropy.

For later convenience we define

$$\Delta\nu \equiv (\sigma_+ - \sigma_-) + (\rho_+ - \tau_{-+}) E_+^2 - (\rho_- - \tau_{+-}) E_-^2. \quad (10)$$

In the previous section it was pointed out that for $Q_{xy}=\nu_{xy}=0$ the mode intensities rapidly approach a stationary equilibrium, so in this case $\psi \rightarrow \Delta\nu \cdot t + \psi_0$ [see Eq. (5)].

Before proceeding with a comparison of experiment and theory it is instructive to consider exactly what it is that one measures in an experiment. We write the two circularly polarized components of the electric field in terms of a rectangular coordinate system:

$$\mathbf{E}_+(t) = E_+[\hat{x}\cos(\nu_+ t + \varphi_+) + \hat{y}\sin(\nu_+ t + \varphi_+)], \quad (11)$$

$$\mathbf{E}_-(t) = E_-[\hat{x}\cos(\nu_- t + \varphi_-) - \hat{y}\sin(\nu_- y + \varphi_-)]. \quad (12)$$

In this form it is easy to show the well-known result that the output of a polarization-insensitive detector, which measures $\langle |\mathbf{E}_+ + \mathbf{E}_-|^2 \rangle$ (the average is taken over an optical period), does not contain any components at the difference frequency of the two modes. The simplest

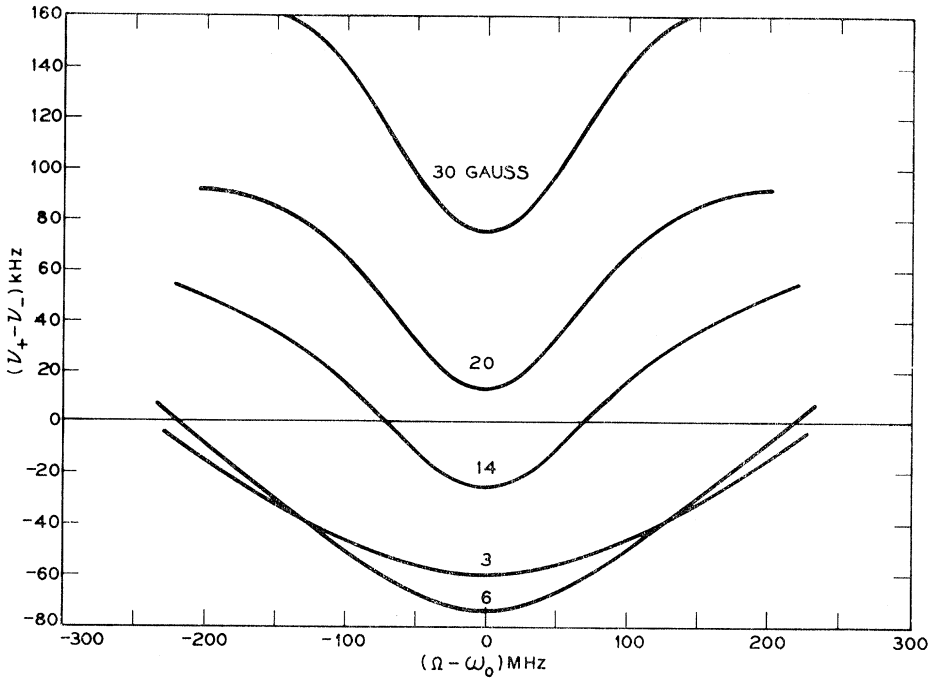

FIG. 7. Theoretical curves of the frequency difference between the oppositely circularly-polarized modes, as functions of cavity detuning, for several values of axial magnetic field. These curves are for a $J=1\rightarrow J=0$ transition. The other constants used in the calculations were: $g_a=1.3$, $\gamma_a/2\pi=20$ MHz, $\gamma_b/2\pi=30$ MHz, $\gamma_{ab}/2\pi=100$ MHz, $Ku=420$ MHz, $\mathfrak{N}=1.375$, $\Delta=577$ MHz, $l=0.007$. The third-order integrals were evaluated using the δ-function approximation. Cavity anisotropy was not included in these calculations.

way to observe this difference frequency is to mix the modes with a linear polarizer, which we will assume has its axis at an angle θ with respect to the x axis. The component of the electric field along the θ direction is given by

$$E_\theta(t)=[\mathbf{E}_+(t)+\mathbf{E}_-(t)]\cdot\hat{e}_\theta$$
$$=E_+\cos(\nu_+t+\varphi_+-\theta)+E_-\cos(\nu_-t+\varphi_-+\theta). \quad (13)$$

If the beam falls on a detector, the output will be proportional to I_θ where

$$I_\theta=\langle E_\theta^2(t)\rangle$$
$$=E_+^2/2+E_-^2/2+E_+E_-\cos(\nu_+t+\varphi_+-\nu_-t-\varphi_--2\theta). \quad (14)$$

Using Eq. (5) we obtain the final result:

$$I_\theta=(E_+^2+E_-^2)/2+E_+E_-\cos(\psi-2\theta). \quad (15)$$

This tells us that for the case we are considering in this section ($\psi\rightarrow\Delta\nu\cdot t+\psi_0$) the output of such a detector will consist of a dc component and a sinusoidal component at a frequency $\Delta\nu$, with the polarizer angle entering only as a phase factor.

In more physical terms, the opposite circular polarizations add to give elliptical polarization. The electric vector of this ellipse rotates in the direction of that of the more intense circular component, and the ellipse rotates in the same direction as the electric vector of the higher-frequency component, with an angular frequency of half the difference of the angular frequencies of the electric vectors of the two components. When viewed through a linear polarizer this rotating ellipse gives a signal at the difference or beat frequency of the two circular components.

As a zeroth approximation, one expects the two polarizations to oscillate with the same frequency since they are on the same resonator mode. The first-order correction to this is the term $(\sigma_+-\sigma_-)$ in Eq. (10), which results from the splitting of the zero-field dispersion curve into two separate curves, one for each polarization. Except for very large detunings this always leads to a positive $\Delta\nu$. (The polarization ellipse spins in the direction given by the direction of the magnetic field and a right-hand rule.) The ρ and τ terms in the frequencies are the third-order corrections, and for sufficiently small fields and detunings they may overcome the effect of the σ terms so as to drive the beat frequency negative.

Typical behavior of the beat frequency as a function of cavity tuning and magnetic field is shown in Figs. 6 and 7. Figure 6 shows experimental curves for a $J=1\rightarrow J=2$ transition, and Fig. 7 shows theoretical curves for a $J=1\rightarrow J=0$ transition. Other investigators have published similar data except that in our experiments we made use of the θ dependence of Eq. (15) to determine the absolute sign of the beat frequency rather than just its magnitude. (This is described in greater detail in the Appendix.) Both figures display the basic features described above.

To compare theory and experiment in more detail it is most convenient to consider the beat frequency as a function of magnetic field with the cavity tuned to line center. Experimental and theoretical curves of this type are given in Figs. 8 and 9 for $J=1\rightarrow J=0$ and $J=1\rightarrow J=2$ transitions, respectively. [We do not observe a beat note until the field is large enough to overcome frequency-locking effects (see Sec. V), and to eliminate any strong coupling (for the $J=1\rightarrow J=0$ transition).]

These curves differ from the mode intensity curves in that they are considerably simpler and in that absolute calibrations are available for both axes. Because of these two facts we ran a number of calculations for different sets of parameters to see how closely we could fit the data without resorting to complicated curve-fitting techniques. We see from Figs. 8 and 9 that the experimental curves can be fairly well described by three parameters: the magnetic field for which the beat frequency is zero, H_0; the maximum negative frequency, F_-; and the slope of the curve in the positive-frequency region, $(\partial F/\partial H)_+$. Since the cavity loss enters the theoretical expressions for the frequencies as a scale factor, and we do not have an independent measure of this loss, we have a certain amount of freedom to adjust the frequency scale on the theoretical calculations to reproduce the experimental values for F_- or $(\partial F/\partial H)_+$. However, the known mirror transmissions and the approximately known maximum gains for the transitions,[14] place definite limits on the range of cavity losses that we can use for this purpose.

Let us first consider the $J=1\rightarrow J=0$ case shown in Fig. 8. From a curve of total output power as a function of cavity tuning we determined the relative excitation ($\mathfrak{N}=1.375$), and an approximate value for $\gamma_{ab}(\gamma_{ab}/2\pi=$ 100 MHz). We then ran calculations for various values of γ_a and γ_b. The best fit with experiment was for $\gamma_a/2\pi=20$ MHz, $\gamma_b/2\pi=30$ MHz, and is shown in the figure. The theoretical curve is plotted for a single pass cavity loss of 0.7%, which was chosen to fit the experimental F_-. If we assume a loss of 0.85% we can fit

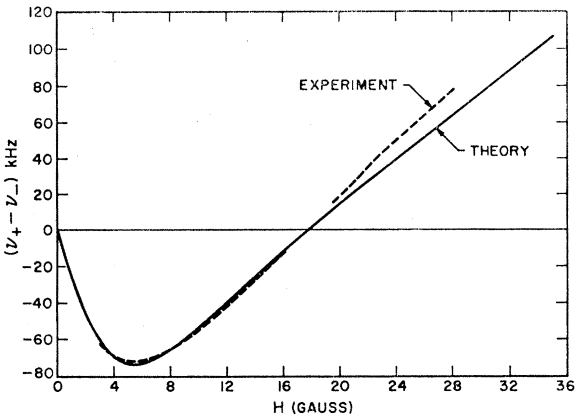

FIG. 8. Experimental and theoretical curves of the frequency difference between the polarization modes as functions of axial magnetic field strength for a $J=1\rightarrow J=0$ transition with the cavity tuned to atomic-line center. The experimental curve is for the same maser used for Fig. 2 except that the total pressure was 1.9 Torr. The constants used in the theoretical calculation were: $J_a=1$, $J_b=0$, $g_a=1.3$, $\gamma_a/2\pi=20$ MHz, $\gamma_b/2\pi=30$ MHz, $\gamma_{ab}/2\pi=100$ MHz, $Ku=420$ MHz, $\mathfrak{N}=1.375$, $\Delta=577$ MHz. The third-order integrals were evaluated using the δ-function approximation. A single-pass cavity loss l of 0.7% was chosen to fit the experimental curve in the negative-frequency region.

[14] W. R. Bennett, Jr., Appl. Opt. Suppl. 1, 38 (1962).

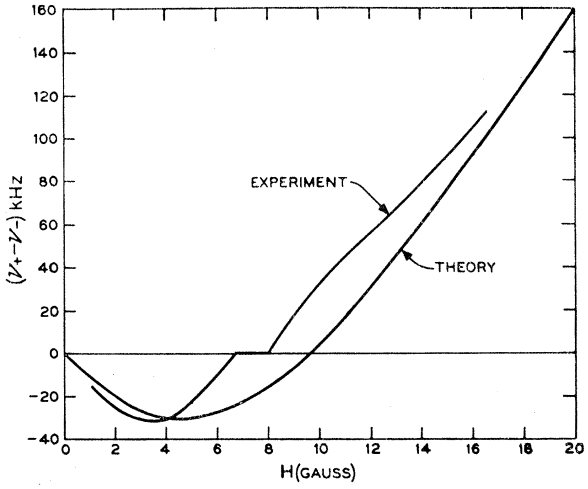

FIG. 9. Experimental and theoretical curves of the frequency difference between the polarization modes as functions of axial magnetic field strength for a $J=1\rightarrow J=2$ transition with the cavity tuned to atomic-line center. The experimental curve is from the same maser used for Fig. 1 except that the total pressure was 2.1 Torr. The constants used in the theoretical calculation were: $J_a=1$, $J_b=2$, $g_a=g_b=1.3$, $\gamma_a/2\pi=18$ MHz, $\gamma_b/2\pi=$ 40 MHz, $\gamma_{ab}/2\pi=120$ MHz, $Ku=1010$ MHz, $\mathfrak{N}=1.16$, $\Delta=1000$ MHz, $l=0.04$. The third-order integrals were evaluated using the δ-function approximation. Cavity anisotropy, which causes the frequency-locking shown in the experimental curve, was not included in the theoretical calculations.

$(\partial F/\partial H)_+$ much more closely, but then the theoretical value for F_- is -87 kHz.

For our mirrors and discharge configuration, losses in the range of 0.7–0.85% appear to be quite reasonable. The value assumed for γ_a is somewhat smaller than that obtained from the magnetic tuning dip, but when we correct for the different pressures used in the two experiments the discrepancy is only about 20%, and does not appear to be particularly significant. (Arbitrarily increasing the coupling strength to that observed in the results on the mode intensities did not appreciably change the calculated frequencies.) At this high excitation one expects some disagreement between experiment and theory because of the neglect of higher-order terms in the theory, but on the whole the agreement seems quite satisfactory.

The situation is rather different when we consider the case of the $J=1\rightarrow J=2$ transition shown in Fig. 9. For the theoretical curve we used the pressure-broadened level widths from Ref. 3, and to fit the observed F_- we needed to assume a single-pass cavity loss of 4.0%. This value for the loss is sufficiently high as to strain credibility, although not so high as to be clearly impossible. However, we were unable to find any set of parameters for which the theoretical curves were in significantly better agreement with experiment than that shown in Fig. 9. For a much smaller γ_a and/or larger γ_{ab} the theoretical value for H_0 is closer to the experimental value, but then it is not possible to fit F_- without assuming an impossibly large loss ($\geq 10\%$), and the ratio $(\partial F/\partial H)_+/F_-$ is much larger than that

found in the experiment. Population differences between the magnetic sublevels, such as were used in the mode-intensity calculations shown in Fig. 1, did not have a significant effect on the frequency calculation. We also ran some calculations in which we arbitrarily increased the coupling coefficients [θ's and τ's in Eqs. (1)–(4)], in an attempt to include the additional coupling found in the mode-intensity results, but the effects on the frequencies were very small.

It is not clear at the present time whether the differences between the experimental and theoretical curves for the $J=1\rightarrow J=2$ transition are the result of a basic inadequacy in the theory, or simply the result of a number of small effects plus our failure to find the "correct" combination of parameters. Since the theory appears to fit the experiment so well for the $J=1\rightarrow J=0$ transition, the disagreement for the $J=1\rightarrow J=2$ transition is all the more puzzling. It appears that this is an area where a detailed curve-fitting approach could be of significant value. Despite this small disagreement, we feel that in general the agreement between theory and experiment is very good.

V. EFFECTS OF CAVITY ANISOTROPY

To include the effects of cavity anisotropy one needs to consider the full set of Eqs. (1) to (5) with Q_{xy} and/or $\nu_{xy}\neq 0$. In general ψ is a periodic function of time so there are no stationary solutions, and in principle one should integrate the three differential equations to determine the equilibrium solutions. This approach has been used, but we find that many of the phenomena can be obtained without numerical integrations if we assume the anisotropy is sufficiently small that the mode amplitudes are essentially constant. (In (II-V) this is referred to as the "decoupled approximation.") In this case we can deal with the single equation

$$\dot{\psi}=\Delta\nu+Q_{xy}\sin\psi(E_+/E_-+E_-/E_+) -\nu_{xy}\cos\psi(E_+/E_--E_-/E_+), \quad (16)$$

which we will write in the simplified form

$$\dot{\psi}=A+B\sin(\psi+\psi_a). \quad (17)$$

In the limit of small B (i.e., $Q_{xy}\rightarrow\nu_{xy}\rightarrow 0$) this equation has the simple solution $\psi=\Delta\nu\cdot t+\psi_0$ and gives us a constant sinusoidal beat note when the two modes are mixed with a linear polarizer, as described in Sec. IV. Lamb[8] has pointed out that an expression of the form of Eq. (17) predicts a frequency locking for $|A|<|B|$. In this case ψ will asymptotically approach $\psi=-\sin^{-1}(A/B)-\psi_a$. These limits have been observed previously. In this paper we are concerned with both the limits and with the region between them.

An exact solution of Eq. (17) will be given below, but before doing that let us consider qualitatively the behavior predicted by the differential equation. As was pointed out in Sec. IV, $\dot{\psi}$ is twice the angular velocity of the rotating polarization ellipse, so this equation tells us that the angular velocity will vary or "pulse" as a function of the polarization orientation. For A and B of the same sign the minimum velocity will come at $\psi+\psi_a=3\pi/2$ and the maximum velocity at $\psi+\psi_a=\pi/2$. For A and B of opposite signs the orientations of maximum and minimum velocity are interchanged. As A approaches B the minimum velocity approaches zero and the maximum velocity approaches B. From this we see that as we approach a locking region ($A\rightarrow B$), the spinning polarization ellipse, which has been spinning at a uniform angular velocity of $A/2$, will begin to spin nonuniformly in such a way that it slows to a minimum angular velocity as it passes the orientation at which it will eventually lock (the locking axis). When $|A|=|B|$ the polarization ellipse will asymptotically approach a constant orientation. If A continues to change in the same direction, this constant orientation will move in the opposite direction to that in which the polarization was spinning until $|A|=|B|$ again, at which point the polarization orientation has moved through about $\pi/2$ (ψ changes by about π). For a further change in A the modes will unlock, and the polarization ellipse will start to spin again with the same characteristics as before, except that it will spin in the opposite direction, and the orientations of maximum and minimum angular velocity will be approximately interchanged. Since A, B, and ψ_a are all functions of the intensities, the orientations of maximum and minimum angular velocity will be somewhat dependent on the mode intensities even when the intensities are not modulated. Hence, as the maser operating point is moved through a locking region the polarization will rotate by about, but not exactly, 90°, and the locking regions on opposite sides of line center will have different locking axes. However, in many cases these effects are sufficiently small that it is still useful to think in terms of the decoupled approximation.[15]

The nonuniform rotation of the polarization ellipse can be seen quite clearly in a rather simple experiment in which one observes the beat note through a polarizer rotating with a period long compared to the period of the beat note, and displays the result on an oscilloscope with a sweep time of the order of the period of the polarizer rotation. Before looking at the experimental results let us consider what we expect to see on the basis of the above qualitative description. To simplify the discussion we will assume that the polarization ellipse is a line, in other words, the light is linearly polarized. We define φ as the angle between the locking axis and the plane of polarization ($\varphi=\psi/2-\varphi_0$), and θ as the angle between the locking axis and the axis of the polarizer. The angle between the plane of polarization and the axis of the polarizer is then ($\varphi-\theta$), so

[15] This complicated time dependence of the polarization can be seen quite clearly in a computer produced movie of the polarization ellipse as a function of time. This movie was shown at the January 1967 meeting of the American Physical Society; see M. Sargent III, W. E. Lamb, Jr., W. J. Tomlinson, and R. L. Fork, Bull. Am. Phys. Soc. **12**, 90 (1967).

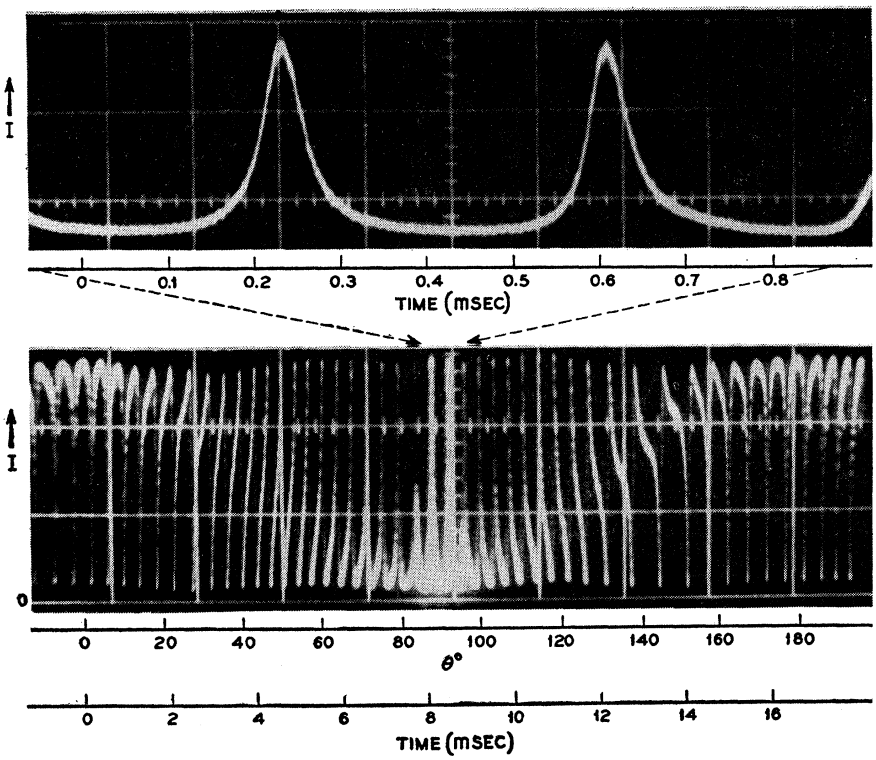

FIG. 10. Experimental results for the maser intensity as a function of time, as observed through a slowly rotating linear polarizer. These results are for the same maser used to obtain the data for Fig. 1 (He–Ne, 0.6328 μ, $J=1\rightarrow J=2$). The maser was tuned about 300 MHz above line center, and was in an axial magnetic field of about 4 G. The upper trace shows the intensified central portion of the lower trace, with a faster sweep rate.

the intensity observed through the polarizer is $I=I_0\cos^2(\varphi-\theta)$. This function is almost periodic with a frequency equal to the beat frequency plus or minus twice the polarizer rotation frequency, so to a first approximation we expect to see a sinusoidal-like variation of the intensity at essentially the beat frequency. When the polarization passes the locking axis ($\varphi=n\pi$), $d\varphi/dt$ will be a minimum so $(d/dt)(\varphi-\theta)$ will also be a minimum. (In some cases it will even be negative.) If the oscilloscope sweep time is many times the period of the beat note, these minimum slope points will be observed mainly as intensified portions of the oscilloscope trace because of the reduced writing rate of the beam. These points will occur when the observed intensity is $I_m=I_0\cos^2(n\pi-\theta)=I_0\cos^2\theta$ so we expect the oscilloscope record to be intensified along the line $I_0\cos^2\theta$.

This intensification is clearly visible in the lower part of Fig. 10 which shows the output intensity as a function of time for a He-Ne maser at 0.6328 μ, as observed through a polarizer rotating at about 30 revolutions per second. (The upper part of the figure shows the central portion of the record with a faster sweep rate to display the wave shape.) As the operating conditions were adjusted to bring the maser closer to single-frequency operation, the intensification along the line $I_0\cos^2\theta$, as shown in Fig. 10, became more and more distinct as the polarization spent more and more time near the locking axis. When the two frequencies finally locked, the pattern on the oscilloscope changed abruptly to the single line $I_0\cos^2\theta$. Since the oscilloscope sweep was synchronized with the polarizer rotation, when we continued to vary the operating conditions in the same direction we observed the rotation of the plane of polarization as a phase shift of the oscilloscope trace. When this phase shift corresponded to a total rotation of the polarization by about 90° the modes unlocked and we again observed a pattern similar to Fig. 10, except that then the intensification was very nearly along the line $I_0\cos^2(\theta+\pi/2)$. Thus this simple experiment readily confirms all the qualitative features predicted from Eq. (17). Figure 10 also provides a test of our assumption that the mode intensities are unmodulated, since any such modulation would show up as variations in the envelope of the beat note. Close examination of the figure reveals that such variations are no more than about 5%, hence our assumption is valid.

For a more quantitative test of the theory we consider the detailed wave shape of the beat note as a function of the polarizer angle. To obtain theoretical curves to compare with experiment we solve Eq. (17). This equation can be integrated analytically, giving, for $|A|>|B|$:

$$\psi(t)+\psi_a=\sin^{-1}\left(\frac{-B+A\sin\Phi}{A-B\sin\Phi}\right), \tag{18}$$

where

$$\Phi=A[1-(B/A)^2]^{1/2}t+\sin^{-1}(B/A), \tag{19}$$

and we have chosen the origin of time such that $\psi(t=0)=-\psi_a$. (Since the inverse sine function is

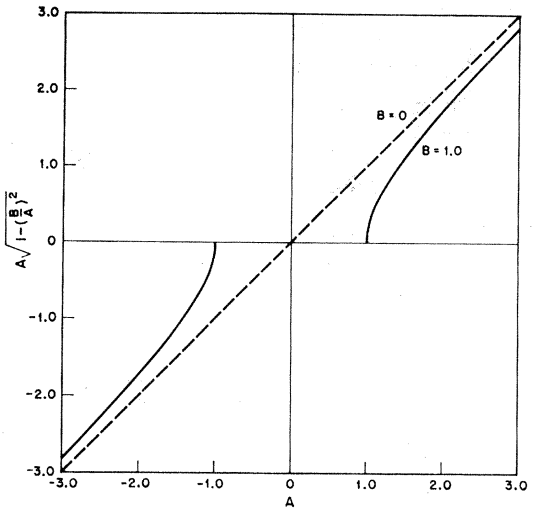

FIG. 11. Plot of the quantity $A\,[1-(B/A)^2]^{1/2}$ as a function of A for two values of B. This figure shows the approximate behavior of the beat frequency near a region of zero beat with ($B\neq 0$) and without ($B=0$) anisotropy in the cavity.

multiple-valued we must be careful to choose the proper value so that ψ is continuous, and $\dot{\psi}$ has the same sign as A.) Substituting Eqs. (18) and (19) into Eq. (15) gives the desired equation for the wave form of the beat note as a function of polarizer angle. Although the wave form is a fairly complicated function of the parameters, we can see at once from Eq. (19) that it is periodic with a frequency of $A[1-(B/A)^2]^{1/2}$, so the anisotropy has the effect of reducing the frequency by a factor of $[1-(B/A)^2]^{1/2}$. In Sec. IV (Figs. 7 to 9) we saw that in the vicinity of locking regions $\Delta\nu$, or A, is usually a fairly linear function of either the cavity tuning or the magnetic field, so that near such regions experimental measurements of the beat frequency as a function of these variables essentially have the form $A[1-(B/A)^2]^{1/2}$ as a function of A. This function is plotted in Fig. 11. From the figure we see that the effect on the frequency is relatively small until we are quite close to the locking region and then the frequency drops very rapidly for small variations in A. This can be seen quite clearly in the experimental curves in Figs. 6 and 9. The experiments are often described by saying that the frequency suddenly "jumps" from some finite value to zero, but in light of the above discussion we can understand the entire phenomenon in terms of continuous processes.

The upper part of Fig. 12 shows experimental results for the beat-note wave shape for five different polarizer orientations. Other investigators have published experimental results for similar wave shapes but, since their data were recorded on oscilloscopes which were triggered by the signals themselves, information was lost as to the relative phases of the wave forms for different polarizer orientations. As shown in Fig. 16 we made use of two detectors, one for observing the wave shape through an adjustable polarizer, and the other for producing a trigger signal for the oscilloscope (see Appendix). The wave-form detector was dc coupled so the zero of intensity is correctly placed, and the fact that the curves have minimum intensities of zero indicated that in Eq. (15) we should set $E_1=E_2$. (The small differences in peak intensities and periods between the various curves are primarily the results of fluctuations in the maser operating conditions over the time required for the measurements.) Since we do not know the actual orientation of the cavity axes, or the ratio ν_{xy}/Q_{xy}, in the theoretical calculations we arbitrarily set $\psi_a=0$, and the empirically determined polarization orientation for minimum $\dot{\psi}$ was labeled $\theta=225°$.

In addition to scale constants, the remaining quantity which is required for the theoretical calculations is the ratio A/B, which indicates the closeness to the locking region. We determined this from the ratio of the half-intensity width of the peak of the $\theta=135°$ curve to the period of the same curve, and obtained a value $A/B=2$. [From Eq. (18) it can be shown that $A/B=\sec(\pi\Delta t/T)$ where Δt is the half-intensity width and T is the period.] Theoretical results using these constants are shown in the lower part of Fig. 12, and are in

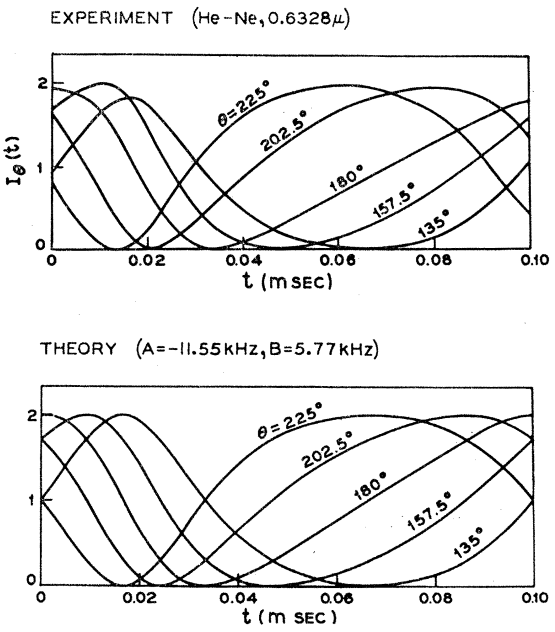

FIG. 12. Experimental and theoretical curves of the beat-frequency wave shape for several orientations of the linear polarizer used to mix the modes. The experimental curves were recorded from the same maser used for the data in Fig. 1 (He–Ne, 0.6328 μ, $J=1\rightarrow J=2$). The detector was dc-coupled, and the oscilloscope was triggered at a constant phase value (see Appendix). The theoretical curves are from Eqs. (15), (18), and (19), with $E_+=E_-=1$, $A=-11.55$ kHz, $B=5.77$ kHz, $\psi_a=0$. The θ origin for the experimental curves was chosen such that the polarization orientation for minimum angular velocity was along the line $\theta=225°$.

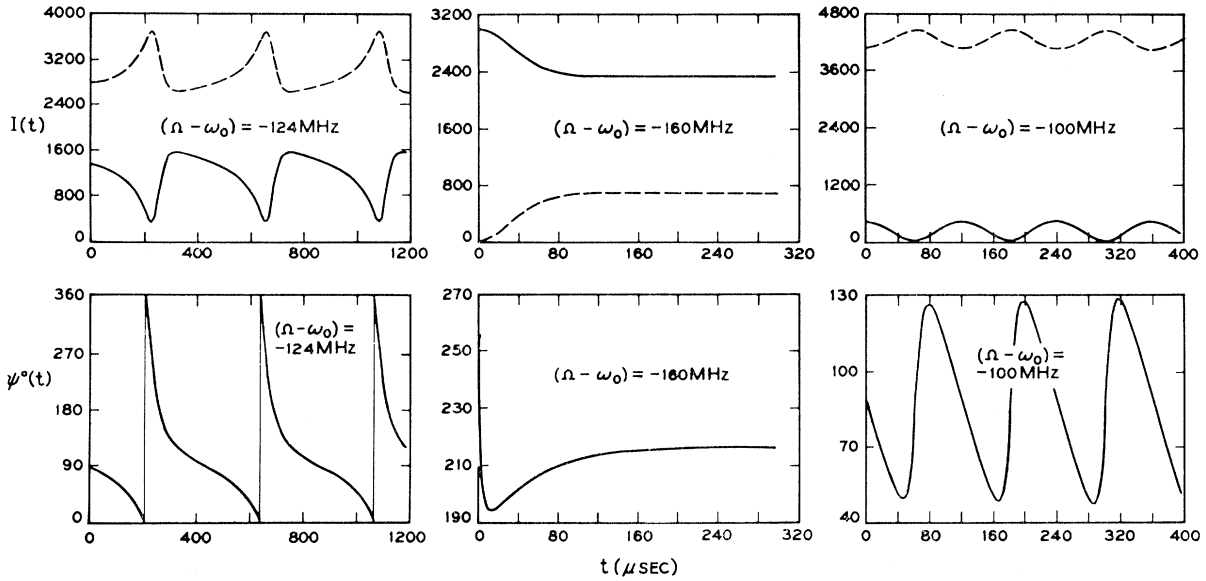

FIG. 13. Theoretical curves of mode intensities and relative phase as functions of time for three different cavity detunings. The constants used in the calculations were: $J_a=1$, $J_b=0$, $g_a=1.3$, $\gamma_a/2\pi=30$ MHz, $\gamma_b/2\pi=60$ MHz, $\gamma_{ab}/2\pi=100$ MHz, $Ku=420$ MHz, $H=2$ G, $\mathfrak{N}=1.2$, $\Delta=577$ MHz, $(l_x+l_y)/2=10^{-2}$. $(l_x-l_y)/2=2\times10^{-5}$, $(\varphi_x-\varphi_y)/2=0$. The third-order integrals were done exactly. These curves are the results of numerical integrations of Eqs. (1)–(5).

excellent agreement with the experimental results. This agreement between the two families of curves indicates that for this case Eq. (17) accurately describes the time dependence of the polarization. Near a locking region the beat frequency is very sensitive to small variations in the cavity length, as seen in Fig. 10, particularly in the region between 11 and 14 msec. This may explain the reported observations of nonharmonically related components in the frequency spectrum of the beat note (i.e., a nonperiodic wave form).[16]

The final phenomena which we consider are the effects of cavity anisotropy on the mode intensities. To obtain theoretical predictions of these effects from Eqs. (1)–(5), we must resort to numerical integration. While this is a fairly straightforward problem, it can easily use large amounts of computer time. Since this calculation makes use of the theory in greater generality, it provides a very sensitive test of the theory, but by the same token, it is also sensitive to errors in the input parameters, and has two more unknown parameters (Q_{xy} and ν_{xy}) than were involved in the previous calculations. Because of this, and the fact that we have already discovered small discrepancies between theory and experiment, we did not attempt a detailed comparison of theory and experiment for these phenomena. We have, however, integrated the theoretical expressions for several cases, and find results which are in surprisingly good agreement with both experiment and the conclusions of the previous section.

Most of the integrations were run for a $J=1\rightarrow J=0$ transition in an axial magnetic field of 2 G. Figure 13 shows the calculated time behavior of the mode intensities and phase difference for three different cavity detunings for $(\varphi_x-\varphi_y)/2=0$ and $(l_x-l_y)/2=2\times10^{-5}$. This value for the magnitude of the anisotropy was chosen on the basis of the results shown in Fig. 12 and is consistent with that predicted by the Fresnel equations for an angle of the order of the mirror tilt necessary to give the desired cavity loss. The curves for a detuning of −124 MHz show the features we expect on the basis of the previous discussion, but the differences are worth emphasizing. The intensity variations of the two modes are essentially negatives of each other, but they are not quite in phase and have slightly different amplitudes so their sum, the total intensity, is modulated at the beat frequency. This is a result of the nonlinearity of the maser medium and indicates that the two modes are not orthogonal. The relatively small modulation of the output indicates that the results could probably be more compactly represented in terms of elliptically polarized almost-orthogonal modes; but we have found it most convenient, both experimentally and computationally, to adhere to the circularly polarized representation. The other difference we would like to point out is that, although $\psi_a=0$, the minimum slope point for ψ comes at about $\psi=85°$, rather than $\psi=90°$ as predicted in the decoupled approximation. For a detuning of −160 MHz the anisotropy is sufficiently strong to lock the two modes to a single frequency, and the figure shows a roughly exponential decay to a stationary equilibrium. The third case shown in Fig. 13, for a detuning of −100 MHz, is a rather interesting com-

[16] W. Culshaw and J. Kannelaud, Phys. Rev. 145, 257 (1966).

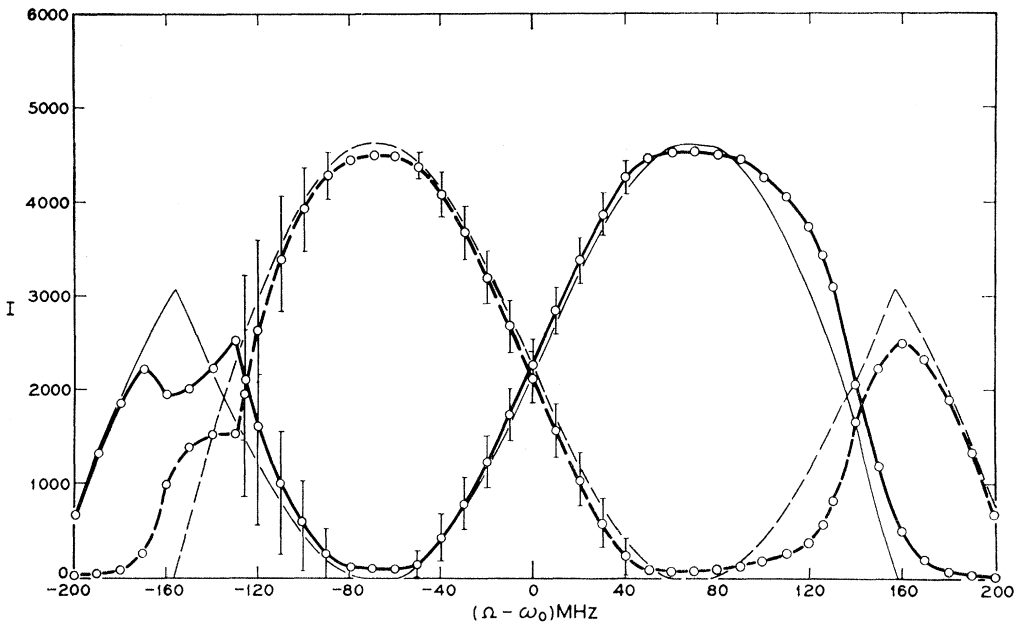

FIG. 14. Theoretical curves of mode intensities as functions of cavity detuning with $Q_{xy}=\nu_{xy}\neq 0$. The calculations are for a $J=1\rightarrow J=0$ transition in an axial magnetic field of 2 G, using the same constants as were used for Fig. 13 except that $(l_x-l_y)/2=(\varphi_x-\varphi_y)/2=\sqrt{2}\times 10^{-5}$, and the δ-function approximation was used for the third-order integrals. The circles indicate calculated equilibrium values of the intensities for those cases where the modes are locked to a common frequency. For those cases where the modes are not locked the vertical bars show the ranges of the modulation of the intensities and the circles show their mean values. The heavy curves have been drawn through the equilibrium or mean values to indicate the pattern which would be observed by a detector with a time constant many times the period of the beat frequency, and should be compared to the 2.4-G experimental results shown in Fig. 2. The light-weight curves are the calculated intensities for an isotropic cavity ($Q_{xy}=\nu_{xy}=0$). The calculations shown in this figure required about 10 min time on an IBM 7094 computer.

bination of the two previous cases. Notice that the phase undergoes a stable oscillation but does not rotate. For the first 40 μsec or so $d\psi/dt$ is negative and the time behavior of the mode intensities is similar to the unlocked case, with the exception that the ratio of the mode intensities is larger. Equation (16) shows that a large intensity ratio has the same effect as a large anisotropy. At about 48 μsec this intensity ratio becomes large enough to cause locking, as we can see from the fact that $d\psi/dt$ changes sign. At this point the time behavior begins to resemble the locked case until about 70 μsec, when the intensity ratio becomes small enough to unlock the modes again as evidenced by the further change in sign of $d\psi/dt$. The computer results indicate that this oscillation is stable.

The experimental results on mode intensities as functions of cavity detuning given in Sec. III do not show any modulation because the time constant of the detection system was much longer than the period of the modulation. To compare the theoretical results with such experiments we must average over the time variations of the theoretical curves. Figure 14 shows the result of such calculations for $(\varphi_x-\varphi_y)/2=(l_x-l_y)/2=\sqrt{2}\times 10^{-5}$. (Since we have no independent measure of the phase anisotropy we have simply set the loss and phase effects equal, and kept the magnitude of the total effect the same as for the previous figure.) For those points where the modes are locked we have indicated the equilibrium intensities by circles. In regions where the modes are unlocked we have indicated the ranges of the intensity variations by vertical bars, with circles to mark the mean values. For this particular set of calculations we did not find any of the oscillating-phase solutions discussed above. The heavy curves drawn through the equilibrium or mean value points are the theoretical predictions to be compared with experiment, and the lightweight curves are theoretical results for the case of an isotropic cavity. From the figure we see that the anisotropy has several effects on the intensities. The most noticeable effects are the marked asymmetry about atomic line center, and the rapid variations in the intensities from -130 to -175 MHz as the maser goes into single-frequency operation. The asymmetry comes from the fact that the loss and phase anisotropy terms have opposite signs on opposite sides of line center [see Eq. (16)]. We also see that the maser goes into single-frequency operation in the regions around ± 75 MHz where the ratio of the mode intensities is very large; however, the resultant state is elliptically polarized rather than circularly polarized as predicted for the isotropic cavity. The point of equal intensities has been shifted from line center to a point

about 2 MHz lower; however, the anisotropy does not change the slopes of the intensities in the central crossover region, which implies that it cannot account for the additional coupling discussed in Sec. III.

Comparing Fig. 14 with the experimental results for a $J=1\rightarrow J=0$ transition in a field of 2.4 G shown in Fig. 2, we find that the experimental curves display all the predicted features. To verify that the modes lock to a common frequency at the points where the intensities show the rapid changes, we used a fast-response detector to observe the beat frequency at the same time as we recorded the intensities with slower-response detectors. In all cases we found that the breaks in the intensities occurred at the edges of locking regions. This was true for either cavity tuning or magnetic field scans, for either of the two transitions investigated. Although no attempt was made to vary parameters to being the theoretical results shown in Fig. 14 into better quantitative agreement with experiment, comparison with Fig. 2 shows that the qualitative agreement is excellent.

Calculations similar to those shown in Fig. 14 but for a $J=1\rightarrow J=2$ transition showed that the theory predicts bumps in the intensities at the edges of the frequency-locking regions, but that these bumps are less pronounced than those in the experimental 3.8-G curve of Fig. 1. For a larger anisotropy the bumps are larger, but the frequency-locking regions are much wider than those observed in the experiments. This would agree with the results of the previous section which indicated that perhaps the theoretical values for the beat frequency are too small for a $J=1\rightarrow J=2$ transition. The reservations stated at that time also apply to this case, but these results reinforce the need for a further careful study of this discrepancy. We wish to emphasize, however, that this discrepancy is a quantitative disagreement; the qualitative features of the experiment are all predicted by the theory.

From our results on the effects of cavity anisotropy, it appears that Eqs. (1)–(5) are of the correct form to predict all the qualitative features of the experiments, and if we adjust the coefficients in the equations, as in Fig. 12, we can usually obtain excellent quantitative agreement with experiment. If we use the theoretical expressions for these coefficients in terms of the basic parameters of the system, we find that for a $J=1\rightarrow J=0$ transition the disagreement between theory and experiment is sufficiently small that it seems reasonable to ascribe it to errors in the parameters used for the calculation. For a $J=1\rightarrow J=2$ transition the disagreement between theory and experiment is sufficiently large that it is difficult to believe that it could be caused solely by such errors. It appears from these results, and from the data on the beat frequency as a function of magnetic field, that for a $J=1\rightarrow J=2$ transition the theoretical expressions underestimate the quantity $\Delta\nu$ [Eq. (10)], and that if this quantity were increased the effects of cavity anisotropy could be predicted by the theory.[17]

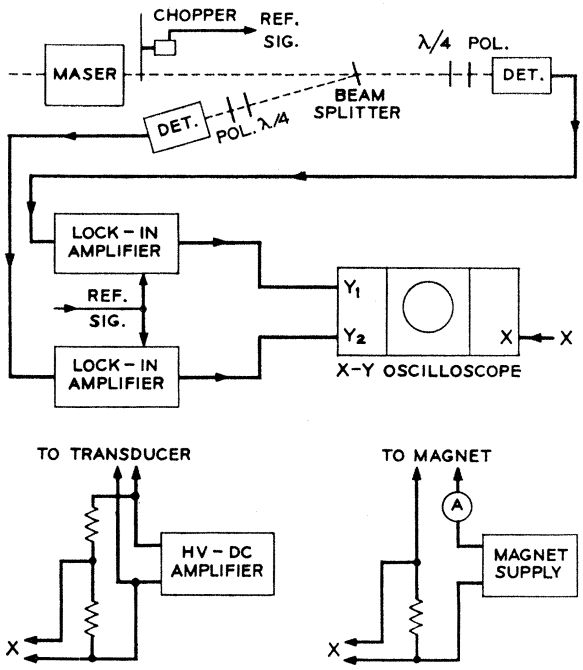

FIG. 15. Block diagram of the equipment used for measurements of mode intensities as functions of cavity tuning or magnetic field.

VI. CONCLUSIONS

The principal conclusion of this paper is that the basic agreement between theory and experiment is very good. Thus, we expect the theory to be quite useful for predicting the behavior of various optical masers in magnetic fields and for obtaining atomic-level parameters from experimental data. The most significant discrepancy, as pointed out in an earlier publication,[5] is the inability of the theory to precisely predict the strength of the coupling between the two polarization modes, particularly as observed in $J=1\rightarrow J=0$ transitions. The other major discrepancy is in the fit to experiment of the calculated frequency difference for the $J=1\rightarrow J=2$ transition. The most dramatic success is the match of the cavity anisotropy effects with those predicted theoretically. This latter success, together with the fact that the very general anisotropy term appears to be unable to account for the coupling discrepancy, suggests that, while the cavity has been well described, the atoms and electric fields have not yet been adequately handled. Since consideration of quan-

[17] It has come to our attention that the thesis of H. de Lang [University of Utrecht, 1966 (unpublished)] contains a very readable treatment of anisotropy phenomena, both in the absence of a magnetic field, and in an axial magnetic field, for weak-coupled transitions. He discusses more general anisotropies than we have considered, but in all his work he uses the decoupled approximation (constant mode intensities), so he is not able to handle the intensity modulation effects shown in Figs. 13 and 14.

tum noise phenomena indicates that noise effects are unlikely to alter the coupling strength,[18] collision phenomena appear, by the process of elimination, to be the most likely source of the additional coupling. Thus, there is a need for additional experimental and theoretical effort directed toward identifying and explaining the effects of atomic collisions in optical masers in magnetic fields.[19]

ACKNOWLEDGMENTS

We wish to acknowledge the considerable help of M. Sargent III who participated in many discussions and made available the bulk of the computer programs used in this work. Mrs. C. A. Lambert and Mrs. M. L. Thomson also assisted greatly in the computational work. W. E. Lamb, Jr., J. P. Gordon, and M. A. Pollack provided many helpful discussions. A. D. White furnished the maser used for the experiments on the 0.6328 μ transition, and L. J. Heilos most ably assisted with the design, fabrication, and alignment of the apparatus.

APPENDIX: DESCRIPTION OF THE EXPERIMENTAL APPARATUS AND PROCEDURES

Masers

Two masers were used in the experiments described in this paper. For the experiments on the 0.6328 μ line we used a dc-excited internal-mirror maser with a mirror spacing of 15 cm, and a 1-mm-diam. capillary discharge region 10 cm long. The mirrors had radii of curvature of 1 m, and multilayer dielectric coatings with transmissions of about 0.4% at the operating wavelength. To prevent undesirable reflections from the back surfaces of the mirrors these were inclined at about 1° to the front surfaces. An annular electrostrictive ceramic (PZT-5) was used to vary the mirror spacing to scan the cavity frequency across the atomic line. The axial magnetic field was provided by a solenoid wound on the capillary section of the discharge tube. Small correction coils were used to improve the field uniformity so that over the entire discharge region the field did not vary by more than $\pm 3\%$, and most of the variation was in the relatively small regions at the ends of the discharge. The solenoid was parallel to the axis of the maser within less than $\pm 0.1°$, and a Mu-metal box was used to shield out external magnetic fields. The maser was permanently connected to a vacuum and gas-handling system so that the pressure and ratio of He to Ne were readily adjustable, and each day's experiments could be done with a clean fill. All the experiments were done with isotopically pure gases (99.99% Ne^{20}, 99.75% He^3). A capacitance manometer was used to measure the gas pressures, and provided a constant monitor on the pressure during the course of an experiment.

The maser used for the experiments on the 1.52 μ line was essentially the same as that used at 0.6328 μ except for its basic dimensions and a few details of the mechanical construction. The mirror spacing was 26 cm, and the capillary region of the discharge tube had a diameter of 2 mm, and was about 20 cm long. The mirror radii of curvature were 2 m. All other details described above were the same for the two masers.

Equipment and Procedures for Polarization Intensity Measurements

The basic equipment used for measurements of the intensities of the circularly polarized modes is shown in Fig. 15. After passing through a mechanical chopper ($\sim$500 Hz), the maser beam was divided into two approximately identical beams by a beam splitter. The beam splitter was used with its normal at an angle of only about 2° from the incident beam so as to minimize its polarizing effects. The two beams then passed through circular polarizers consisting of mica $\lambda/4$ plates followed by linear polarizers (Polaroid-type HR), and were detected in PbS detectors. Interference filters were used to isolate the maser radiation. The signals from the detectors were demodulated in standard commercial "lock-in" amplifiers (P.A.R. Model JB-5) and used to drive the two inputs of a dual-channel preamp in the vertical section of a Tektronix-type RM564 storage oscilloscope. To calibrate the relative sensitivities of the two detection channels one of the polarizers was rotated 90° so that both channels were sensitive to the same circular polarization, and the gains of the channels were adjusted to give equal outputs. With the polarizer rotated back to its original position the channels then had equal sensitivities for their preferred polarizations.

The ceramic transducer used to vary the cavity length was connected across the output of a high-voltage dc-amplifier, which was driven by a standard function generator and/or a manually adjustable bias circuit. A resistive voltage divider across the ceramic provided a low-voltage signal which was a roughly linear function of the cavity frequency. This signal was used to drive the horizontal section of the storage oscilloscope for displays of mode intensities as functions of cavity tuning.

[18] J. P. Gordon (private communication).

[19] *Note added in proof:* We have recently succeeded in demonstrating that collision-induced transitions between magnetic sublevels are, as proposed above and in our earlier letter [Ref. 5], the origin of the strong coupling in $J=1\rightarrow J=0$ transitions. We have incorporated such collisions in the theory in terms of different decay rates for the various multipole moments of the $J=1$ state, and obtain very good agreement with experiment. Our observations are in agreement with Hanle effect experiments on other atomic systems by W. Happer and E. B. Saloman [Phys. Rev. **160**, 23 (1967)]. The relationship between the work of Happer and Saloman and the laser problem has also been noted by D. Polder and W. Van Haeringen [Phys. Letters **25A**, 337 (1967)].

Equipment and Procedures for Beat-Frequency Measurements

For most measurements of the beat frequency the setup was as shown in Fig. 15 except that a fast-response detector (Type 7102 photomultiplier for 0.6328 μ, InSb detector for 1.52 μ) was used to observe, through a linear polarizer, the beam from the other end of the maser. The output from the fast detector was displayed on an oscilloscope, and its frequency counted by a Hewlett-Packard Model 5245L frequency counter. A digital-to-analog converter was used to convert the output of the counter into a voltage proportional to frequency which was then plotted on an X-Y recorder as a function of either magnetic field or cavity tuning.

The above equipment measures the absolute value of the frequency difference, $|\psi|$, but does not tell us which mode has the higher frequency. To determine the sign of the beat note we used the arrangement shown in Fig. 16. The detector and polarizer (#1) on the left are the same as were used to measure the magnitude of the beat note. The detector and polarizer on the right (#2) provide a reference signal to trigger the oscilloscope at a constant phase angle. This setup provides records such as those shown in Fig. 12. Notice that in Fig. 12 in addition to the change in wave form as a function of the angle of polarizer #1 there is also a phase shift such that for increasing θ the peak of the wave form appears at earlier times. This indicates that the polarization ellipse, and hence the electric vector of the higher-frequency mode, were rotating in the opposite direction to that in which the polarizer was being rotated. In this way we obtain a simple and direct measurement of the senses of rotation of the modes. We merely find the direction of rotation of polarizer #1 which causes the oscilloscope display to move to the right. This is then the direction of rotation of the electric vector of the higher-frequency mode.

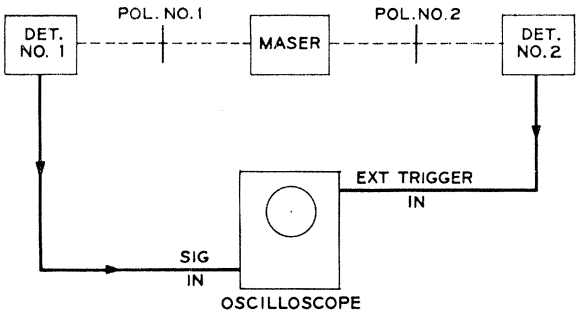

FIG. 16. Block diagram of the equipment used to measure the absolute sign of the beat frequency.

For the results shown in Fig. 10 polarizer #1 was rotated by a synchronous motor, and the oscilloscope was triggered by the input wave form to the motor. In this way the oscilloscope is triggered at a constant polarizer orientation.

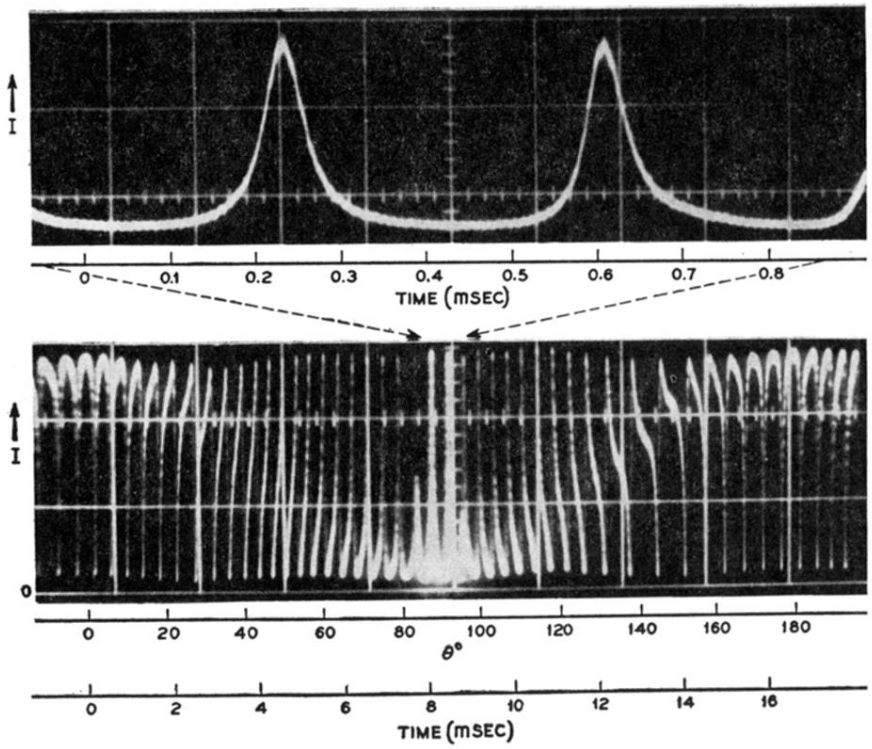

FIG. 10. Experimental results for the maser intensity as a function of time, as observed through a slowly rotating linear polarizer. These results are for the same maser used to obtain the data for Fig. 1 (He–Ne, 0.6328 μ, $J=1\rightarrow J=2$). The maser was tuned about 300 MHz above line center, and was in an axial magnetic field of about 4 G. The upper trace shows the intensified central portion of the lower trace, with a faster sweep rate.